Ternary Rare Earth Metal Silicides $RE_2RE'_3Si_4$ with Orthorhombic Sm_5Ge_4 or Tetragonal Zr_5Si_4 Type Structure

Ute Ch. Rodewald[a], Birgit Heying[a], Dirk Johrendt[b], Rolf-Dieter Hoffmann[a], and Rainer Pöttgen[a]

[a] Institut für Anorganische und Analytische Chemie, Westfälische Wilhelms-Universität Münster, Wilhelm-Klemm-Straße 8, D-48149 Münster, Germany
[b] Department Chemie, Ludwig-Maximilians-Universität München, Butenandtstraße 5 – 13 (Haus D), D-81377 München, Germany

Reprint requests to R. Pöttgen. E-mail: pottgen@uni-muenster.de

Z. Naturforsch. **59b,** 174 – 181 (2004); received December 12, 2003

Dedicated to Professor Ingo-Peter Lorenz on the occasion of his 60th birthday

Ternary silicides $RE_2RE'_3Si_4$ (RE = La, Ce; RE' = Y, Lu) were synthesized by arc-melting of the elements. Single crystals were grown by annealing the arc-molten buttons slightly below the melting points in water-cooled silica tubes in an induction furnace. Five silicides $RE_2RE'_3Si_4$ were investigated by X-ray powder and single crystal diffraction: Zr_5Si_4 type, $P4_12_12$, $a = 779.4(3)$, $c = 1441.3(9)$ pm, $wR2 = 0.072$, 1806 F^2 values, 45 variables for $La_{1.72(4)}Y_{3.28(4)}Si_4$, $P4_32_12$, $a = 769.92(7)$, $c = 1412.3(1)$ pm, $wR2 = 0.079$, 1846 F^2 values, 45 variables, BASF = 0.36(4) for $La_{1.72(2)}Lu_{3.28(2)}Si_4$, $P4_12_12$, $a = 778.6(1)$, $c = 1433.9(3)$ pm, $wR2 = 0.054$, 1910 F^2 values, 46 variables, BASF = 0.34(4) for $Ce_{1.82(6)}Lu_{3.18(6)}Si_4$, $P4_32_12$, $a = 778.8(3)$, $c = 1436.0(10)$ pm, $wR2 = 0.166$, 1916 F^2 values, 45 variables for $Ce_{1.71(7)}Y_{3.29(7)}Si_4$, and Sm_5Ge_4 type, $Pnma$, $a = 749.2(2)$, $b = 1484.2(7)$, $c = 780.3(2)$ pm, $wR2 = 0.070$, 1956 F^2 values and 49 variables for $Ce_{1.47(3)}Y_{3.53(3)}Si_4$. The local coordinations of both structure types are very similar, *i. e.* CN 18, 16, and 14 coordination polyhedra for the $RE1$, $RE2$, and $RE3$ atoms. The main structural motif is the eightfold coordination of the $RE3$ positions by rare earth metal atoms. These slightly distorted $RERE'_8$ cubes are condensed *via* common corners (Zr_5Si_4 type) or *via* common edges (Sm_5Ge_4 type). All silicon atoms in these silicides form Si_2 pairs at Si–Si distances ranging from 254 to 258 pm. DFT band structure calculations confirm the metallic character of both silicides and the trivalent state of cerium in Ce_5Si_4. The COHP analysis (Crystal Orbital Hamilton Population) of the Si–Si bonds shows a significant occupation of Si–Si antibonding orbitals, which is partially compensated by a Si–Si $\pi*$, $\sigma* \rightarrow$ Y-4d (Ce-5d) back donation.

Key words: Silicide, Crystal Structure, Solid State Synthesis, Chemical Bonding

Introduction

Intermetallic cerium compounds of the type $Ce_xT_yX_z$ (T = transition metal; X = element of the 3rd, 4th or 5th main group) have attracted considerable interest in recent years due to their strongly varying magnetic and electrical properties [1]. Cerium can adopt the $4f^\circ$ (Ce^{4+}) or $4f^1$ (Ce^{3+}) state or even a non-integral valence. Besides simple antiferromagnetically or ferromagnetically ordered ground states Fermi liquid, heavy Fermion, or Kondo type behavior has been observed for this large family of compounds. The crystal chemistry of the $Ce_xT_yX_z$ compounds is rather complex, however, most structures have a common feature. The T and X atoms build a three-dimensional polyanionic network in which the cerium atoms fill cages or distorted pentagonal or hexagonal channels.

Many of the $Ce_xT_yX_z$ intermetallics have only one crystallographic cerium site. This is especially the case for most of the equiatomic $CeTX$ compounds. A survey of the literature is given in [2]. With such a single cerium site, the magnetic response of the cerium ions is uniform. If two or more crystallographically independent cerium sites occur, the magnetic behavior can be more complex. The multiplicity and the local coordina-

Table 1. Crystal data and structure refinement for $La_{1.72(4)}Y_{3.28(4)}Si_4$, $La_{1.72(2)}Lu_{3.28(2)}Si_4$, $Ce_{1.82(6)}Lu_{3.18(6)}Si_4$, $Ce_{1.71(7)}Y_{3.29(7)}Si_4$ and $Ce_{1.47(3)}Y_{3.53(3)}Si_4$.

Empirial formula	$La_{1.72(4)}Y_{3.28(4)}Si_4$	$La_{1.72(2)}Lu_{3.28(2)}Si_4$	$Ce_{1.82(6)}Lu_{3.18(6)}Si_4$	$Ce_{1.71(7)}Y_{3.29(7)}Si_4$	$Ce_{1.47(3)}Y_{3.53(3)}Si_4$
Molar mass	642.91 g/mol	927.71 g/mol	923.78 g/mol	644.61 g/mol	632.44 g/mol
Structure type	Zr_5Si_4	Zr_5Si_4	Zr_5Si_4	Zr_5Si_4	Sm_5Ge_4
Lattice parameters (Guinier data)	$a = 779.4(3)$ pm	$a = 769.92(7)$ pm	$a = 778.6(1)$ pm	$a = 778.8(3)$ pm	$a = 749.2(2)$ pm $b = 1484.2(7)$ pm
	$c = 1441.3(9)$ pm	$c = 1412.3(1)$ pm	$c = 1433.9(3)$ pm	$c = 1436.0(10)$ pm	$c = 780.3(2)$ pm
	$V = 0.8755$ nm^3	$V = 0.8372$ nm^3	$V = 0.8692$ nm^3	$V = 0.8710$ nm^3	$V = 0.8676$ nm^3
Formula units per cell	$Z = 4$	$Z = 4$	$Z = 4$	$Z = 4$	$Z = 4$
Space group	$P4_12_12$ (No. 92)	$P4_32_12$ (No. 96)	$P4_12_12$ (No. 92)	$P4_32_12$ (No. 96)	*Pnma* (No. 62)
Calculated density	4.88 g/cm^3	7.36 g/cm^3	7.06 g/cm^3	4.92 g/cm^3	4.84 g/cm^3
Crystal size	$15 \times 30 \times 40$ μm^3	$15 \times 40 \times 60$ μm^3	$10 \times 20 \times 25$ μm^3	$20 \times 30 \times 50$ μm^3	$8 \times 20 \times 50$ μm^3
Transmission (max : min)	1.56	2.00	1.89	1.57	1.85
Absorption coefficient	30.2 mm^{-1}	47.8 mm^{-1}	45.6 mm^{-1}	30.9 mm^{-1}	31.4 mm^{-1}
Detector distance	60 mm	–	60 mm	60 mm	60 mm
Exposure time	20 min	–	12 min	35 min	20 min
ω Range; increment	0 – 180°, 1.0°	–	0 – 180°, 1.0°	0 – 180°, 1.0°	0 – 180°, 1.0°
Integr. param. A, B, EMS	14.0, 4.0, 0.016	–	14.5, 4.5, 0.016	10.5, 1.7, 0.017	14.0, 4.0, 0.014
$F(000)$	1128	1552	1549	1134	1116
θ Range	2 to 35°	3 to 35°	3 to 35°	2 to 35°	2 to 35°
Range in *hkl*	±12, ±12, ±22	±12, ±12, ±22	±12, ±12, ±23	±12, ±12, ±23	±12, ±23, ±12
Total no. reflections	12590	12692	13121	13194	12343
Independent reflections	1806 ($R_{int} = 0.063$)	1846 ($R_{int} = 0.124$)	1910 ($R_{int} = 0.078$)	1916 ($R_{int} = 0.085$)	1956 ($4R_{int} = 0.113$)
Reflections with $I > 2\sigma(I)$	1669 ($R_{sigma} = 0.029$)	1499 ($R_{sigma} = 0.066$)	1540 ($R_{sigma} = 0.051$)	1693 ($R_{sigma} = 0.040$)	1416 ($R_{sigma} = 0.063$)
Data/restraints/parameters	1806 / 0 / 45	1846 / 0 / 45	1910 / 0 / 46	1916 / 0 / 45	1956 / 0 / 49
Goodness-of-fit on F^2	0.873	1.032	0.941	1.064	1.012
Final R indices $[I > 2\sigma(I)]$	$R1 = 0.029$	$R1 = 0.038$	$R1 = 0.035$	$R1 = 0.062$	$R1 = 0.041$
	$wR2 = 0.070$	$wR2 = 0.072$	$wR2 = 0.051$	$wR2 = 0.159$	$wR2 = 0.064$
R Indices (all data)	$R1 = 0.033$	$R1 = 0.059$	$R1 = 0.052$	$R1 = 0.071$	$R1 = 0.071$
	$wR2 = 0.072$	$wR2 = 0.079$	$wR2 = 0.054$	$wR2 = 0.166$	$wR2 = 0.070$
Extinction coefficient	0.0010(2)	0.00012(8)	0.00042(5)	0.0072(9)	0.0008(1)
Twin ratio; BASF	–	0.36(4)	0.34(4)	–	–
Flack parameter	0.003(12)	–	–	0.04(3)	–
Largest diff. peak and hole	1.00 and −1.25 e/Å^3	2.70 and −3.74 e/Å^3	1.68 and −2.59 e/Å^3	2.58 and −1.99 e/Å^3	1.71 and −1.51 e/Å^3

tion of cerium (position within the three-dimensional T_xX_z network) play an important role. To give some examples, in Ce_2Sn_5 [3] with two cerium sites, magnetic ordering is detected for one site at 3 K, while the other site exhibits valence fluctuation behavior [4]. The indide $Ce_5Ni_6In_{11}$ [5] has a two-fold and an eight-fold cerium position. Both positions show antiferromagnetic ordering, the 2*c* site at 0.63 K and the 8*k* site at 1.1 K [6, 7]. The U_3Si_2 type silicide Ce_3Si_2 [8] has a four-fold and a two-fold cerium site. In contrast to $Ce_5Ni_6In_{11}$, both sites order magnetically at the same temperature [9].

In view of the manifold magnetic behavior it is interesting to try substitutions of one cerium site by a diamagnetic rare earth element, *i. e.* scandium, yttrium, or lutetium. The scattering power of cerium and (Sc, Y, Lu) is sufficiently different so that the substitution effects can reliably be determined from high-angle X-ray intensities. For cerium/lanthanum substitutions it is impossible to examine the occupancies on the basis of X-ray data.

Some recent examples for such substitution effects are the silicides Ce_2YSi_2 and Ce_2ScSi_2 [9], where the magnetic ordering temperature is reduced with respect to binary Ce_3Si_2. More complicated is the situation for Ce_5Si_4 [10] with Zr_5Si_4 type structure which contains three crystallographically different cerium sites. Flandorfer *et al.* [11] started a more systematic investigation of the Ce-Y-Si system in order to study the cerium valence in Ce_5Si_4 as a function of cerium concentration. They refined the structure of CeY_4Si_4 on the basis of X-ray powder data and reported on susceptibility measurements for ternary compounds $Ce_{5-x}Y_xSi_4$.

We have recently synthesized various silicides also in other solid solution systems, *i. e.* $Ce_{5-x}Lu_xSi_4$, $La_{5-x}Lu_xSi_4$, and $La_{5-x}Y_xSi_4$. Depending on the composition, the diamagnetic rare earth elements show different occupancies on the lanthanum (cerium) po-

Table 2. Atomic coordinates and isotropic displacement parameters for $La_{1.72(4)}Y_{3.28(4)}Si_4$, $La_{1.72(2)}Lu_{3.28(2)}Si_4$, $Ce_{1.82(6)}Lu_{3.18(6)}Si_4$, $Ce_{1.71(7)}Y_{3.29(7)}Si_4$, and $Ce_{1.47(3)}Y_{3.53(3)}Si_4$.

Atom	Wyckoff position	occup.	*x*	*y*	*z*	U_{eq}[a]
$La_{1.72(4)}Y_{3.28(4)}Si_4$; space group $P4_12_12$ (No. 92)						
M1	8*b*	0.83(1)La/0.17(1)Y	0.99031(4)	0.35826(4)	0.20894(2)	101(1)
M2	8*b*	0.03(1)La/0.97(1)Y	0.13931(6)	0.01059(6)	0.37575(4)	95(2)
Y	4*a*	1.0	0.18263(7)	*x*	0	94(2)
Si1	8*b*	1.0	0.2900(2)	0.0636(2)	0.1885(1)	107(3)
Si2	8*b*	1.0	0.3471(2)	0.2958(2)	0.3100(1)	127(3)
$La_{1.72(2)}Lu_{3.28(2)}Si_4$; space group $P4_32_12$ (No. 96)						
M1	8*b*	0.86(1)La/0.14(1)Lu	0.00700(9)	0.64798(8)	0.78841(3)	70(2)
Lu1	8*b*	1.0	0.85516(6)	0.99382(7)	0.62431(4)	67(1)
Lu2	4*a*	1.0	0.82142(7)	*x*	0	66(1)
Si1	8*b*	1.0	0.7101(5)	0.9423(5)	0.8131(2)	70(6)
Si2	8*b*	1.0	0.6451(5)	0.7062(5)	0.6870(2)	96(6)
$Ce_{1.82(6)}Lu_{3.18(6)}Si_4$; space group $P4_12_12$ (No. 92)						
M1	8*b*	0.76(1)Ce/0.24(1)Lu	0.99215(7)	0.35757(7)	0.20990(3)	99(1)
M2	8*b*	0.15(1)Ce/0.85(1)Lu	0.14007(5)	0.00839(6)	0.37588(4)	97(1)
Lu	4*a*	1.0	0.18190(6)	*x*	0	103(1)
Si1	8*b*	1.0	0.2907(4)	0.0627(4)	0.1879(2)	93(5)
Si2	8*b*	1.0	0.3488(4)	0.2938(4)	0.3117(2)	113(5)
$Ce_{1.71(7)}Y_{3.29(7)}Si_4$; space group $P4_32_12$ (No. 96)						
M1	8*b*	0.78(2)Ce/0.22(2)Y	0.00964(8)	0.64036(9)	0.79154(4)	176(2)
M2	8*b*	0.08(2)Ce/0.92(2)Y	0.8617(1)	0.9888(1)	0.62391(8)	170(3)
Y	4*a*	1.0	0.8169(1)	*x*	0	159(3)
Si1	8*b*	1.0	0.7087(4)	0.9358(4)	0.8113(2)	180(6)
Si2	8*b*	1.0	0.6550(4)	0.7034(4)	0.6898(2)	195(6)
$Ce_{1.47(3)}Y_{3.53(3)}Si_4$; space group *Pnma* (No. 62)						
M1	8*d*	0.69(1)Ce/0.31(1)Y	0.02209(5)	0.09691(2)	0.82109(5)	95(1)
M2	8*d*	0.05(1)Ce/0.95(1)Y	0.18100(6)	0.12255(3)	0.32175(7)	84(2)
Y	4*c*	1.0	0.3481(1)	1/4	0.9868(1)	79(2)
Si1	4*c*	1.0	0.2304(3)	1/4	0.6232(3)	102(4)
Si2	4*c*	1.0	0.9753(3)	1/4	0.1096(3)	106(4)
Si3	8*d*	1.0	0.1472(2)	0.9606(1)	0.5298(2)	111(3)

[a] U_{eq} (pm^2) is defined as one third of the trace of the orthogonalized U_{ij} tensor.

sitions. The structure refinements of $La_{1.72}Y_{3.28}Si_4$, $La_{1.72}Lu_{3.28}Si_4$, $Ce_{1.82}Lu_{3.18}Si_4$, $Ce_{1.71}Y_{3.29}Si_4$, and $Ce_{1.47}Y_{3.53}Si_4$ are reported herein.

Experimental Section

Synthesis

Starting materials for the preparation of the ternary silicides were ingots of the rare earth elements (Johnson-Matthey) and silicon pieces (Wacker), all with stated purities better than 99.9%. The larger rare earth metal ingots were mechanically cut into smaller pieces under paraffin oil and cleaned with *n*-hexane. Both the paraffin oil and n-hexane were dried over sodium wire. The small rare earth metal pieces were subsequently arc-melted under an atmosphere of *ca.* 600 mbar argon [12]. The argon was purified before over molecular sieves, silica gel, and titanium sponge (900 K). The pre-melting procedure for the rare earth metals strongly reduces a shattering of these elements during the strongly exothermic reaction with silicon. The two rare earth metals and silicon were then mixed in the 2:3:4 atomic ratio and the five silicides were synthesized by arc-melting of the elements. The orthorhombic cerium yttrium silicide was prepared with the starting composition 1.5:3.5:4. The samples were then turned over and remelted in order to achieve homogeneity.

For the La/Y and the La/Lu silicide, single crystals were already obtained after the arc-melting procedure, whereas the Ce/Lu and both Ce/Y samples remained polycrystalline after arc-melting. The buttons were then sealed in evacuated silica tubes and annealed slightly below the melting point in a special water-cooled sample chamber [13] in an induction furnace (Hüttinger TIG 2.5 / 300 or 5.0 / 300) for three hours. Compact pieces of the silicides are light gray with metallic luster. The samples are stable in moist air. No decomposition was observed after several months.

X-ray film data, structure refinements, and EDX

The polycrystalline products have been characterized through their Guinier powder pattern. The Guinier camera was equipped with an image plate system (Fujifilm, BAS-1800) and monochromated Cu-$K_{\alpha 1}$ radiation. α-quartz ($a = 491.30$, $c = 540.46$ pm) was used as an internal standard. The orthorhombic and tetragonal lattice parameters (Table 1) were obtained from least-squares fits of the powder data.

Table 3. Interatomic distances (pm) in the structures of $La_{1.72(4)}Y_{3.28(4)}Si_4$ ($P4_12_12$) and $Ce_{1.47(3)}Y_{3.53(3)}Si_4$ (*Pnma*). The symbol M accounts for the rare earth metal mixing (see Table 2). All distances of the first coordination spheres are listed. Standard deviations are all equal or less than 0.3 pm.

$La_{1.72(4)}Y_{3.28(4)}Si_4$				$Ce_{1.47(3)}Y_{3.53(3)}Si_4$			
M1:	1	Si2	307.7	M1:	1	Si3	308.5
	1	Si1	314.2		1	Si3	313.6
	1	Si1	316.4		1	Si1	315.9
	1	Si2	317.6		1	Si1	318.2
	1	Si2	321.3		1	Si3	318.4
	1	Si1	328.9		1	Si2	321.7
	1	Y	363.2		1	Y	355.4
	1	Y	363.9		1	Y	357.8
	1	Si2	371.3		1	Si3	365.1
	1	M2	376.9		1	M2	376.4
	1	M2	380.4		1	M2	380.0
	1	M2	392.7		2	M1	390.7
	2	M1	392.9		1	M2	394.4
	1	M1	402.0		1	M1	402.2
	1	M2	406.6		1	M2	409.2
	1	M2	410.2		1	M2	410.2
	1	M2	422.9		1	M1	454.4
M2:	1	Si2	288.5	M2:	1	Si3	289.3
	1	Si2	290.9		1	Si3	291.1
	1	Si1	297.2		1	Si2	294.9
	1	Si1	297.5		1	Si2	295.4
	1	Si2	298.8		1	Si3	298.6
	1	Si1	302.3		1	Si1	304.1
	1	Y	342.7		1	Y	346.1
	1	Y	343.1		1	Y	346.8
	1	M1	376.9		1	M1	376.4
	1	M1	380.4		1	M2	378.3
	1	M2	385.2		1	M1	380.0
	1	M1	392.7		2	M2	391.0
	1	M2	398.4		1	M1	394.4
	1	M1	406.6		1	M1	409.2
	1	M1	410.2		1	M1	410.2
	1	M1	422.9	Y:	1	Si2	295.3
Y:	2	Si1	299.1		1	Si1	297.0
	2	Si1	310.6		1	Si1	299.0
	2	Si2	314.5		2	Si3	314.5
	2	M2	342.7		1	Si2	329.1
	2	M2	343.1		2	M2	346.1
	2	M1	363.2		2	M2	346.8
	2	M1	363.9		2	M1	355.4
					2	M1	357.8

The correct indexing of the patterns was ensured through intensity calculations [14] taking the atomic positions from the structure refinements. The lattice parameters determined from the powders and the single crystals agreed well.

Irregularly shaped single crystals of $\sim La_2Y_3Si_4$, $\sim La_2Lu_3Si_4$, $\sim Ce_2Lu_3Si_4$, and two different samples of $\sim Ce_2Y_3Si_4$ were isolated from the as cast or the inductively annealed samples by mechanical fragmentation. They were first examined on a Buerger precession camera equipped with an image plate system (Fujifilm BAS-1800) in order to establish both symmetry and suitability for intensity data collection. Single crystal intensity data of the $\sim La_2Lu_3Si_4$ crystal were collected at room temperature making use of a four-circle diffractometer (CAD4) with graphite monochromatized Mo-K_α radiation (71.073 pm) and a scintillation counter with pulse height discrimination. The scans were performed in the $\omega/2\theta$ mode. An empirical absorption correction was applied on the basis of psi-scan data. Intensity data of all other crystals were collected at room temperature by use of a Stoe IPDS-II diffractometer with graphite monochromatized Mo-K_α radiation (71.073 pm) in oscillation mode. Numerical absorption corrections were applied to the data. All relevant details concerning the data collections and the data treatments are listed in Table 1.

Careful analyses of the data sets revealed the space groups $P4_12_12$ (or $P4_32_12$) and *Pnma* as expected for Zr_5Si_4 [15] and Sm_5Ge_4 [16] type compounds, respectively. The starting atomic parameters were then deduced from automatic interpretations of direct methods with SHELXS-97 [17] and the five structures were refined using SHELXL-97 (full-matrix least-squares on F_o^2) [18] with anisotropic atomic displacement parameters for all sites. In the first refinement cycles the rare earth sites were refined exclusively with the scattering power of lanthanum or cerium. These refinements readily showed that some of the displacement parameters were either too low or to high, indicating a different occupancy for these sites. We then carefully refined the occupancy parameters and allowed La/Y, La/Lu, Ce/Lu, and Ce/Y mixing in the subsequent cycles. These refinements showed, that one site in each compound is fully occupied with yttrium or lutetium, while one or even the two other sites showed mixing of the rare earth metals. These mixed occupancies were refined as

Table 3 (continued).

$La_{1.72(4)}Y_{3.28(4)}Si_4$				$Ce_{1.47(3)}Y_{3.53(3)}Si_4$			
Si1:	1	Si2	255.7	Si1:	1	Si2	258.2
	1	M2	297.2		1	Y	297.0
	1	M2	297.5		1	Y	299.0
	1	Y	299.1		2	M2	304.1
	1	M2	302.3		2	M1	315.9
	1	Y	310.6		2	M1	318.2
	1	M1	314.2	Si2:	1	Si1	258.2
	1	M1	316.4		2	M2	294.8
	1	M1	328.9		1	Y	295.3
Si2:	1	Si1	255.7		2	M2	295.4
	1	M2	288.5		2	M1	321.7
	1	M2	290.9		1	Y	329.1
	1	M2	298.8	Si3:	1	Si3	253.9
	1	M1	307.7		1	M2	289.3
	1	Y	314.5		1	M2	291.1
	1	M1	317.6		1	M2	298.6
	1	M1	321.3		1	M1	308.5
	1	M1	371.3		1	M1	313.6
					1	Y	314.5
					2	M1	318.4

a least-squares variable in the final cycles, while the other occupancies were kept at the ideal values. Refinement of the correct handedness of the tetragonal structures was ensured through refinement of the Flack parameters [19, 20]. The La/Lu and the Ce/Lu crystals showed twinning by inversion. The final difference Fourier syntheses revealed no significant residual peaks (see Table 1). The positional parameters and interatomic distances are listed in Tables 2 and 3. Listings of the observed and calculated structure factors are available*.

The single crystals were coated with a carbon film and analyzed in a Leica 420 I scanning electron microscope by energy dispersive X-ray analyses using LaB_6, CeO_2, yttrium, and SiO_2 as standards. The compositions of the crystals determined by the EDX analyses were in good agreement with those obtained from the structure refinements. No impurity elements heavier than sodium could be detected.

Electronic band structure calculations

Self-consistent *ab initio* band structure calculations were performed with the LMTO method in its scalar relativistic version (program LMTO-ASA 47) [21]. A detailed description may be found elsewhere [22 – 26]. Reciprocal space integrations were performed with the tetrahedron method by using 75 (Y_5Si_4, *Pnma*) or 48 (Ce_5Si_4, $P4_12_12$) irreducible *k*-points within the Brillouin zones [27]. The basis sets consisted of $5s/\{5p\}/4d/\{4f\}$ for Y, $6s/\{6p\}/5d/4f$ for Ce and $3s/3p/\{3d\}$ for Si. Orbitals given in braces were treated by the downfolding technique [28]. To achieve space filling within the atomic sphere approximation, interstitial spheres were introduced to avoid too large overlap of the atom centered spheres. The empty sphere positions and radii were calculated by using an automatic procedure developed by Krier [29]. The COHP (Crystal Orbital Hamiltonian Population) method was used for the bond analysis [30]. COHP gives the energy contributions of all electronic states for a selected bond. The values are negative for bonding and positive for antibonding states. With respect to the well-known COOP diagrams, we plot −COHP(E) to obtain positive values for bonding states.

Discussion

The coordination polyhedra of the two structure types are presented in Fig. 1. They show many similarities. The *M*1 atoms (*M* denotes the La/Y, La/Lu, Ce/Lu, and Ce/Y mixing) of both structure types have

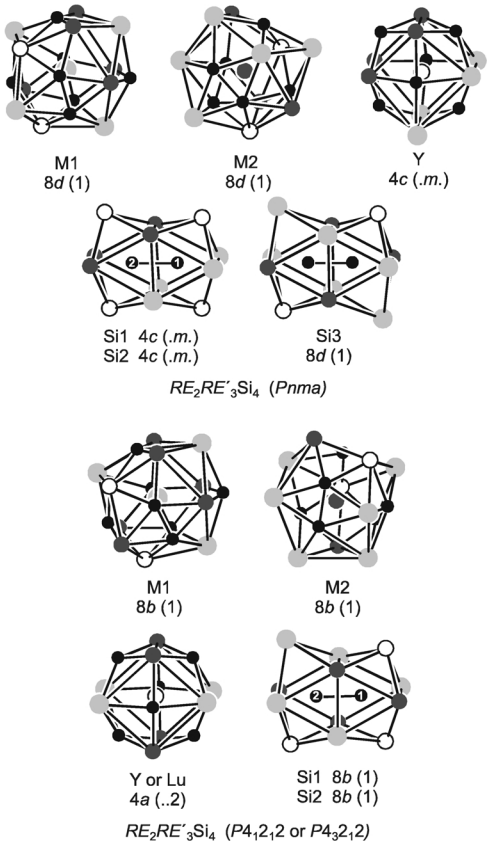

Fig. 1. Coordination polyhedra in the structures of the silicides $RE_2RE'_3Si_4$ (space group *Pnma*) and $RE_2RE'_3Si_4$ (space group $P4_12_12$ or $P4_32_12$). The *RE*1 (M1), *RE*2 (M2), yttrium(lutetium), and silicon sites are drawn as light gray, dark gray, open, and small filled circles, respectively. The site symmetries are indicated.

coordination number (CN) 18 with seven silicon and eleven rare earth metal atoms in their coordination shell. A similar situation occurs for the *M*2 atoms. They have both the lower CN 16 with six silicon and ten rare earth metal neighbors. It is worthwhile to note that the *M*2 site in the $La_{1.72}Lu_{3.28}Si_4$ crystal is fully occupied by lutetium, in contrast to all other crystals investigated.

The third rare earth position in the two structure types has the much smaller CN 14 with eight rare earth metal neighbors in a slightly distorted cubic coordination. The six square faces of this coordination polyhedron are capped by silicon atoms. The low coordination number is most likely the reason for the full occupancy of these sites with the much smaller yttrium and

*Details may be obtained from: Fachinformationszentrum Karlsruhe, D-76344 Eggenstein-Leopoldshafen (Germany), by quoting the Registry No's. CSD-413569 ($La_{1.72}Y_{3.28}Si_4$), CSD-413570 ($La_{1.72}Lu_{3.28}Si_4$), CSD-413571 ($Ce_{1.82}Lu_{3.18}Si_4$), CSD-413573 ($Ce_{1.71}Y_{3.29}Si_4$), and CSD-413572 ($Ce_{1.47}Y_{3.53}Si_4$).

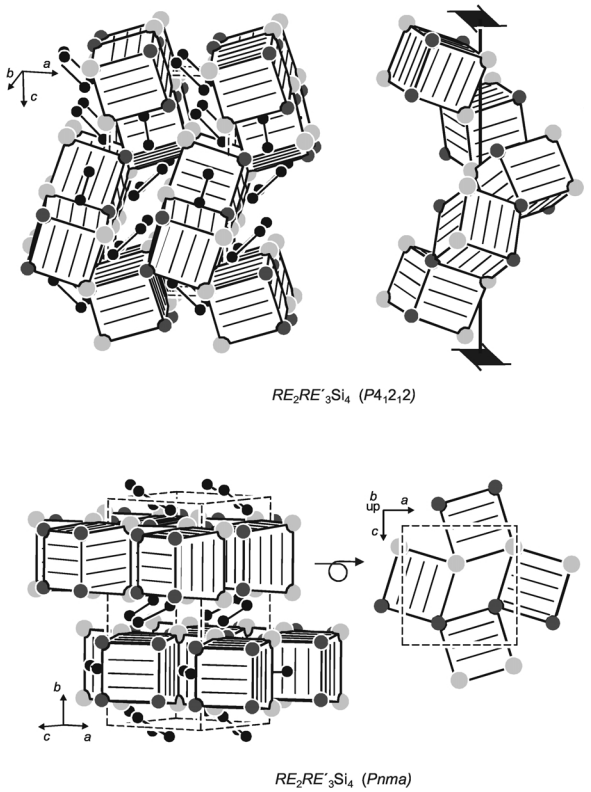

Fig. 2. The structures of $RE_2RE'_3Si_4$ (space group *Pnma*) and $RE_2RE'_3Si_4$ (space group $P4_12_12$ or $P4_32_12$). The distorted cubes around the *RE*3 positions and the Si_2 dumb-bells are emphasized. The mixed rare earth metal, yttrium(lutetium), and silicon sites are drawn as light gray, medium gray, and black circles, respectively.

lutetium atoms. Although the coordination of the rare earth metal atoms looks quite similar for both structure types at first sight, they are significantly different. This is obvious from Fig. 2 where we show the condensation of the YM_8, respectively LuM_8 cubes. In the tetragonal Zr_5Si_4 type structure, the cubes are condensed *via* common corners, forming a complicated three-dimensional network. As emphasized at the upper right-hand part of Fig. 2, they are arranged around the 4_1 screw axis. In the orthorhombic Sm_5Ge_4 type silicides the cubes are condensed *via* common edges forming layers in the *ac* planes around $y = 1/4$ and $y = 3/4$. These are the mirror planes of space group *Pnma*.

Within the solid solution $Ce_{5-x}Y_xSi_4$ [11] the structure type changes from the Zr_5Si_4 to the Sm_5Ge_4 type for $x \geq\sim 3.5$, according to our X-ray data. With the smaller yttrium atoms, the silicides adopt the orthorhombic Sm_5Ge_4 type as Y_5Si_4 [10] does. The homogeneity range was investigated for the Ce/Y system by Flandorfer *et al.* [11].

Now we focus on the coordination of the silicon atoms. They have also very similar coordination in both structure types. Each silicon atom has CN 9 in a tri-capped trigonal prismatic coordination (Fig. 1). Since all silicon atoms form pairs, these trigonal prisms are condensed *via* a rectangular face.

Depending on the structure type and the size of the rare earth element, the Si–Si distances show a small variation. In the crystals investigated, they range from 254 to 258 pm, somewhat longer than that in the diamond structure of elemental silicon (235 pm) [31]. At this point it is worthwhile to compare the single crystal data reported here with the X-ray powder data for orthorhombic CeY_4Si_4 determined by Flandorfer *et al.* [11]. There is a severe discprepancy for the Si–Si distances: 226 pm Si3–Si3 and 271 pm Si1–Si2 for the powder data as compared to 254 pm Si3–Si3 and 258 pm Si1–Si2 for our single crystal. Since the distance of 226 pm determined from the powder data is significantly shorter than that in elemental silicon, we assume that this is an artifact of the powder refinement. In most ternary silicides the Si–Si distances are longer than in elemental silicon. This is also the case for the silicides $Sc_3Pr_2Si_4$, $Sc_{1.26}Pr_{3.74}Si_4$, and $Sc_{3.96}Nd_{1.04}Si_4$ with the same orthorhombic structure [32].

Assuming essentially trivalent rare earth elements and Si–Si single bonds within these silicides, electron counting in the binaries can be written to a first approximation as $(5Ce^{3+})^{15+}(2\ Si_2{}^{6-})^{12-} \cdot 3e^-$ and $(5Y^{3+})^{15+}(2\ Si_2{}^{6-})^{12-} \cdot 3e^-$. This leaves three electrons per formula unit for the conduction band, in agreement with the results of the DFT band structure calculation. As seen from the DOS curves shown in Figs. 3 and 5, both silicides exhibit a remarkable density of states at the Fermi level (E_F) confirming the metallic character. The DOS at E_F is strikingly high for both compounds and mainly composed of partially filled dd-σ-orbitals of yttrium or cerium, respectively, forming strong Y–Y and Ce–Ce bonding. In the case of Ce_5Si_4, also the Ce $4f$-levels contribute significantly to the DOS at E_F. Spin polarized calculations assuming a $4f^1$-configuration of Ce^{3+} converged to a theoretical magnetic spin moment of $0.62\mu_B$/Ce which corresponds to an effective moment $\mu_{eff} = 2.89\mu_B$. The ex-

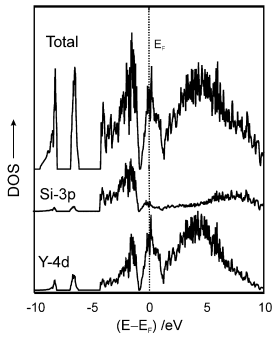

Fig. 3. The total density of states (DOS) of Y_5Si_4 and the contributions of the Si-3*p*- and Y-4*d* orbitals, respectively. The energy zero is taken at the Fermi level.

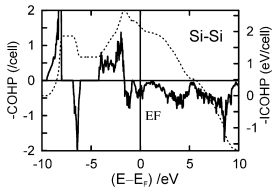

Fig. 4. COHP diagram of the Si-Si bonds in Y_5Si_4. The dotted line represents the integration (ICOHP).

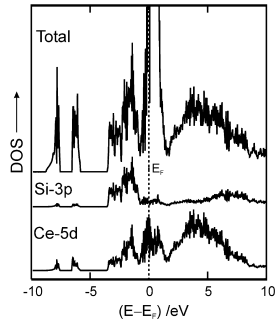

Fig. 5. The total density of states (DOS) of Ce_5Si_4 and the contributions of the Si-3*p*- and Ce-5*d* orbitals, respectively. The energy zero is taken at the Fermi level.

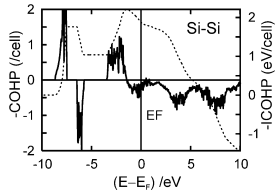

Fig. 6. COHP diagram of the Si-Si bonds in Ce_5Si_4. The dotted line represents the integration (ICOHP).

pected value for the fully polarized $4f^1$-state of Ce^{3+} is $2.54\mu_B$. We can assume that this deviation is due to the known shortcomings in the description of strongly localized $4f$-states within the LSDA rather than an indicator for an intermediate valence state of cerium. In any case, the calculated magnetic ground state justifies the assumption that cerium is essentially trivalent in Ce_5Si_4.

Figs. 4 and 6 show the COHP diagrams of the Si–Si bonds in Y_5Si_4 and Ce_5Si_4. The graphs of the two crystallographically different Si–Si bonds in Y_5Si_4 are almost identical and therefore merged in Fig. 4. In both cases we find Si–Si antibonding levels below and in the vicinity of the Fermi level. In this energy range, the DOS is dominated by the *d*-levels of yttrium or cerium. A similar bonding picture was drawn for the Si–Si pairs in Eu_5Si_3 [33], where the Si–Si $\pi*$ bands are completely filled. These $\pi*$-levels overlap with the Eu-5*d* bands and a Si–Si $\pi* \rightarrow$ Eu-5*d* back donation becomes evident. Eu_5Si_3 is formally a valence compound according to $(5Eu^{2+})^{10+}Si^{4-}\ (Si_2)^{6-}$, but Ce_5Si_4 and Y_5Si_4 contain three excess electrons in the unit cell: $(5Y^{3+})^{15+}(2\ Si_2{}^{6-})^{12-} \cdot 3e^-$. This leads to an increased occupation of Si–Si antibonding orbitals up to the lowest Si–Si $\sigma*$ bands (Figs. 4 and 6). Since Si–Si $\pi*$ and $\sigma*$ are in the range of the Y-4*d* or Ce-*d* bands, we can also state a Si–Si $\pi*$, $\sigma* \rightarrow$ Y-4*d* (Ce-*d*) back donation, which clearly stabilizes the structure of these silicides.

Acknowledgments

We thank H.-J. Göcke for the work at the scanning electron microscope. This work was financially supported by the Fonds der Chemischen Industrie and by the Deutsche Forschungsgemeinschaft.

[1] A. Szytuła, J. Leciejewicz, Handbook of Crystal Structures and Magnetic Properties of Rare Earth Intermetallics, CRC Press, Boca Raton (1994).
[2] R. Kraft, R. Pöttgen, D. Kaczorowski, Chem. Mater. **15**, 2998 (2003).
[3] S. K. Dhar, K. A. Gschneidner (Jr.), O. D. McMasters, Phys. Rev. B **35**, 3291 (1987).
[4] A. P. Murani, Physica B **230 – 232**, 259 (1997).
[5] Ya. M. Kalychak, P. Yu. Zavalii, V. M. Baranyak, O. V. Dmytrakh, O. I. Bodak, Kristallografiya **32**, 1021 (1987).

[6] I. Tang, K. A. Gschneidner (Jr.), S. J. White, M. R. Roser, T. J. Goodwin, L. R. Corruccini, Phys. Rev. B **52**, 7328 (1995).
[7] K. A. Gschneidner (Jr.), V. K. Pecharsky, Physica B **223 & 224**, 131 (1996).
[8] E. I. Gladyshevskii, Iz. Akad. Nauk. SSSR 706 (1965).
[9] S. K. Dhar, P. Manfrinetti, A. Palenzona, Y. Kimura, M. Kozaki, Y. Onuki, T. Takeuchi, Physica B **271**, 150 (1999).
[10] G. S. Smith, A. G. Tharp, Q. Johnson, Acta Crystallogr. **22**, 940 (1967).
[11] H. Flandorfer, J. Gröbner, A. Kostikas, C. Godart, P. Rogl, V. Psicharis, A. Saccone, R. Ferro, G. Effenberg, J. Alloys Compd. **297**, 129 (2000).
[12] R. Pöttgen, Th. Gulden, A. Simon, GIT Labor-Fachzeitschrift **43**, 133 (1999).
[13] D. Niepmann, Yu. M. Prots', R. Pöttgen, W. Jeitschko, J. Solid State Chem. **154**, 329 (2000).
[14] K. Yvon, W. Jeitschko, E. Parthé, J. Appl. Crystallogr. **10**, 73 (1977).
[15] H.-U. Pfeifer, K. Schubert, Z. Metallkd. **57**, 884 (1966).
[16] G. S. Smith, Q. Johnson, A. G. Tharp, Acta Crystallogr. **22**, 269 (1967).
[17] G. M. Sheldrick, SHELXS-97, Program for the Determination of Crystal Structures, University of Göttingen, Germany (1997).
[18] G. M. Sheldrick, SHELXL-97, Program for Crystal Structure Refinement, University of Göttingen, Germany (1997).
[19] H. D. Flack, G. Bernadinelli, Acta Crystallogr. **A55**, 908 (1999).
[20] H. D. Flack, G. Bernadinelli, J. Appl. Crystallogr. **33**, 1143 (2000).
[21] O. K. Andersen, Tight-Binding LMTO Vers. 47c, Max-Planck-Institut für Festkörperforschung, Stuttgart (1994).
[22] O. K. Andersen, Phys. Rev. **B12**, 3060 (1975).
[23] O. Jepsen, O. K. Andersen, Phys. Rev. Lett. **53**, 2571 (1984).
[24] O. K. Andersen, O. Jepsen, Z. Phys. **B97**, 35 (1995).
[25] H. L. Skriver, The LMTO Method, Springer, Berlin (1984).
[26] O. Jepsen, M. Snob, O. K. Andersen, Linearized Band-Structure Methods in Electronic Band-Structure and its Applications, Springer Lecture Notes, Springer, Berlin (1987).
[27] O. K. Andersen, O. Jepsen, Solid State Commun. **9**, 1763 (1971).
[28] W. R. L. Lambrecht, O. K. Andersen, Phys. Rev. **B34**, 2439 (1986).
[29] G. Krier, O. Jepsen, O. K. Andersen, unpublished results.
[30] R. Dronskowski, P. Blöchl, J. Phys. Chem. **97**, 8617 (1993).
[31] J. Donohue, The Structures of the Elements, Wiley, New York (1974).
[32] B. Ya. Kotur, O. E. Banakh, R. Černý, J. V. Pacheco Espejel, J. Alloys Compd. **260**, 157 (1997).
[33] R. Pöttgen, R.-D. Hoffmann, D. Kußmann, Z. Anorg. Allg. Chem. **624**, 945 (1998).